Assessment of membrane scaling in pilot-scale nanofiltration process

Yongsun Jang, Sengmin Park, Yongjun Choi, Sangho Lee*

*School of Civil and Environmental Engineering, Kookmin University, Jeongneung-Dong, Seongbuk-Gu, Seoul 136-702, Korea,
Tel. +82-2-910-4529; Fax: +82-2-910-4939; email: sanghlee@kookmin.ac.kr (S. Lee)*

ABSTRACT

This study presents membrane fouling due to scale formation in a pilot-scale nanofiltration (NF) process for industrial wastewater reclamation. The scale formation mechanisms were investigated by applying model equations based on the surface crystallization and bulk crystallization. The longitudinal variations of the local flux, flux, permeability loss, and pressure loss in the membrane modules were also analyzed using the model. The pilot plant consisted of two stages NF systems with the total water production capacity of 50 m^3/d. Since the raw wastewater contains high concentrations of Ca^{2+} and SO_4^{2-} ions, gypsum scale formation occurred during the NF processing. As the scaling potential of brine was different, NF membrane elements in the 2nd stage exhibited faster fouling rates than those did in the 1st stage. In the 2nd stage, the fouling mechanism due to scale formation was identified as surface blockage by surface crystallization rather than cake formation by bulk crystallization.

Keywords: Reverse osmosis; Scale formation; Pilot plant; Fouling; Model

1. Introduction

Water reuse is becoming inevitable as a promising way to provide sustainable water supply in principal applications including agriculture, industry, and indirect and non-potable uses [1–4]. It has attracted great attention from many countries all over the world [5,6]. Climate change appears to worsen the current status of water scarcity and thus acts as a major driver for widespread implementation of water reuse [7]. A key technology for water reuse is membrane process, which removes contaminants in the wastewater to enable the beneficial use of treated water [2,3,6,8]. Reverse osmosis (RO) and nanofiltration (NF) are two typical membrane processes that can remove dissolved ions and organic matters from the wastewater [9], which is essential for industrial water reuse [4,10–12]. They are also used for zero liquid discharge where no discharge is left over [10].

However, industrial water reuse by RO or NF may suffer from problems associated with membrane fouling due to inorganic scale formation [13,14]. Scale formation has been regarded by many researchers and engineers as a critical problem not only in RO/NF [15] but also in other industrial equipments such as evaporator, heat exchanger, and pipes [16]. Scales are mineral precipitates that are formed from solutions saturated or supersaturated with inorganic salts such as calcium sulfate ($CaSO_4$), calcium carbonate ($CaCO_3$), and silica (SiO_2). Scale formation has several adverse impacts on RO/NF membrane processes, including a reduction in flux and water production, a decrease in ion rejection, and shortened membrane life span [13].

To control RO/NF fouling due to scale formation, it is essential to understand its mechanism. It has been reported that there are two distinct mechanisms for scale formation, including surface (heterogeneous) crystallization and bulk (homogeneous) crystallization [17–20]. In the case of the surface crystallization, the formation of inorganic scales is initiated on the membrane surface and the subsequent growth of scales occurs to block the membrane surface [17]. Since these surface crystals are impermeable, the effective surface area of the membrane decreases with a progress of scale formation. In the case of the bulk crystallization, the scale formation

* Corresponding author.

begins in the bulk phase of the solution due to the homogeneous nucleation and thus suspended crystal particles are created [20]. Then, these crystals deposit on the membrane surface by the permeation drag and form cake layer on the membrane surface. Unlike the surface scales, these cake layers are not completely impermeable.

Although several studies have been attempted to analyze the scale formation in RO/NF systems [17,21–24], they mainly focused on bench-scale systems, which have inherent limitations to be applied to pilot- or full-scale membrane processes. In this context, this study intended to explore the effect of scale formation in pilot-scale NF process for water reuse. A simple model was applied to consider the longitudinal variation of the local flux, salt concentration, and fouling in the membrane modules. Using the model, the performance of a pilot-scale NF process was analyzed and the dominant mechanism for scale formation was identified. The originality of this study is to apply the scale formation model to a pilot-scale NF system and analyze the fouling mechanisms and local properties of the membranes.

2. Model development

In this study, we have applied the resistance-in-series model incorporated with the crystallization theory to analyze RO fouling due to scale formation. Unlike previous works, we developed the model for pilot- and full-scale RO plants. In addition, we compared two models based on different crystallization mechanisms to identify which is dominant.

If the surface blockage is the dominant mechanisms for scale formation, the permeate flux is given by:

$$J = \frac{\Delta P - \pi - \Delta P_{loss}}{\eta R_m} \times \frac{A - A_b}{A} \qquad (1)$$

where ΔP is the transmembrane pressure; π is the osmotic pressure; $\Delta P_{loss} = \gamma m_d/S$ is the pressure drop in the membrane channel; η is the permeate viscosity; R_m is the membrane resistance; A is the membrane area; $A_b = \beta m_s$ is the membrane area occupied by surface crystals; S is the cross-section area for membrane channel; γ is the constant for membrane channel blockage; β is the area occupied per unit mass; and m_s is the weight of scale formed directly on membrane surface.

On the other hand, the permeate flux given by the cake filtration model is:

$$J = \frac{\Delta P - \pi - \Delta P_{loss}}{\eta \left(R_m + R_c \right)} \qquad (2)$$

where $R_c = \alpha m_c/A$ is the resistance due to cake formation; α is the specific cake resistance; and m_c is the accumulated weight of precipitated scale.

Based on the crystallization kinetics, the m_s, m_c, and m_d are given by:

$$\frac{dm_s}{dt} = k_s(c_w - c_s)^n = k_s c_s(c_w/c_s - 1)^n \qquad (3)$$

$$\frac{dm_c}{dt} = k_c(c_b - c_s)^n = k_c c_s(c_b/c_s - 1)^n \qquad (4)$$

$$\frac{dm_d}{dt} = k_d(c_b - c_s)^n = k_d c_s(c_b/c_s - 1)^n \qquad (5)$$

where c_w is the wall concentration of solute; c_b is the bulk concentration of solute; c_s is the saturation concentration; n is the reaction order; and k_s, k_c, and k_d are reaction constants for surface blockage, cake formation, and channel blockage. For continuous NF system where the concentration at each position is almost constant, the mass of crystals is assumed to be proportion to operation time.

Combining Eqs. (1), (3), and (5), flux decline due to surface blockage is given by:

$$J = \frac{\Delta P - \pi - \dfrac{k_d c_s (c_b/c_s - 1)^n t}{S}}{\eta R_m} \times \left(1 - \frac{\beta k_s c_s (c_w/c_s - 1)^n t}{A} \right) \qquad (6)$$

In the continuous operation, c_b is assumed to be constant. Thus, Eq. (6) can be simplified as:

$$J = \frac{\Delta P - \pi - r_3 t}{\eta R_m} \times \left(1 - r_1 t \right) \qquad (7)$$

where $r_3 = k_d c_s(c_b/c_s - 1)^n/S$ and $r_1 = \beta k_s c_s(c_w/c_s - 1)^n/A$. Similarly, flux decline due to cake formation is given by combining Eqs. (2), (4), and (5):

$$J = \frac{\Delta P - \pi - \dfrac{k_d c_s (c_b/c_s - 1)^n t}{S}}{\eta \left(R_m + \dfrac{\alpha k_c c_s (c_b/c_s - 1)^n t}{A} \right)} = \frac{\Delta P - \pi - r_3 t}{\eta \left(R_m + r_2 t \right)} \qquad (8)$$

where $r_2 = \alpha k_c c_s(c_b/c_s - 1)^n/A$. Once the flux is calculated, the recovery is given by:

$$\text{Rec} = JA/Q_{in} = Q_{out} + JA \qquad (9)$$

In the model fit, the r_1, r_2, and r_3 were used as the model fit parameters. The data of the pressure drop were first fitted to the model equation to determine r_3. Then, the model fits were carried out using Eqs. (6) and (7) for two different scale formation mechanisms. The results of the model fits were compared to determine the dominant scale formation mechanism in each case.

2.1. Analysis of local flux in pilot scale NF processes

The conventional RO/NF normalization method does not consider the local distribution of flux and salt transport. Only the average values of feed water concentration, applied pressure, and flux are considered. Accordingly, it is difficult to get detailed information on RO process related to these local properties.

To overcome this restriction, a new normalization technique based on the RO transport model was applied. The solution–diffusion equations modified with the thin-film model was applied to predict NF performance as well as permeate quality. Then, the model was fitted to the pilot plant data to estimate water and solute permeability values. Moreover, the changes in local flux and permeate total dissolved solids (TDS) were calculated for in-depth analysis of the NF plant. Details on this model are available in the previous studies [25,26].

3. Experimental setup

3.1. Feed water and membrane

An industrial wastewater after chemical precipitation with lime was used as the feed water. This wastewater contains high concentration of Ca^{2+}, K^+, and SO_4^{2-}. According to the calculation by ROSA software (Dow, USA), the saturation degrees for $CaSO_4$ and CaF_2 were calculated to 58.7% and 2,392%, respectively. This suggests that fouling due to scale formation by $CaSO_4$ occurs at the permeate recovery higher than 33%. Although CaF_2 was already supersaturated, its impact may be lower than that of $CaSO_4$ due to its low solubility. The average water quality is given in Table 1.

The NF membrane elements used in this pilot plant was SU-620 from Toray Industry, Japan. The average rejection percentages for NaCl and $MgSO_4$ were 55.00% and 99.00%, respectively. The maximum pressure for the operation was 14.75 bar. The recommended flow rate of the recirculation flow was 10–16 m^3/d.

3.2. Pilot plant

A schematic diagram for the NF pilot plant is shown in Fig. 1. The raw wastewater was pretreated by the chemical precipitation using lime and the cartridge filter. Then, the feed water was delivered to the 1st stage and 2nd stage NF processes. The membrane areas for the 1st and 2nd stage NF

Table 1
Average compositions of wastewater after chemical precipitation

Ca^{2+} (mg/L)	292
K^+ (mg/L)	539
Na^+ (mg/L)	145
SO_4^{2-} (mg/L)	1,630
Cl^- (mg/L)	43.2
F^- (mg/L)	7.85
TDS (mg/L)	2,657

processes were 54 and 54 m^2, respectively. The 1st stage was operated in a batch mode and the 2nd stage was operated in a continuous mode with recirculation. The recovery ratios for the 1st and 2nd stages were 50% and 60%, respectively,
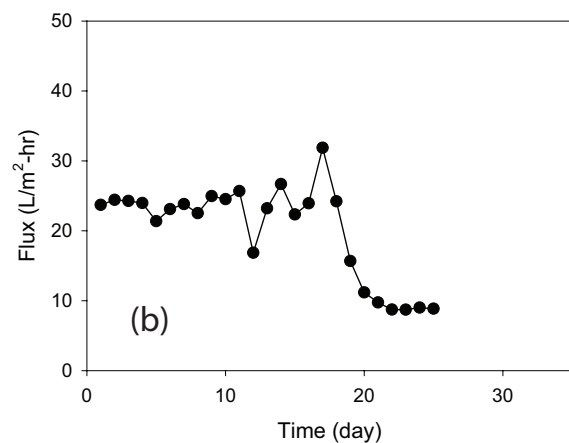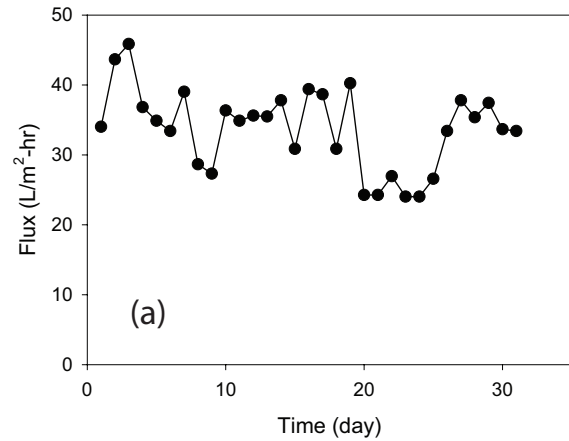

Fig. 2. Changes in flux with operation time in the 1st and 2nd stage NF systems. Flux in the (a) 1st stage and (b) 2nd stage.
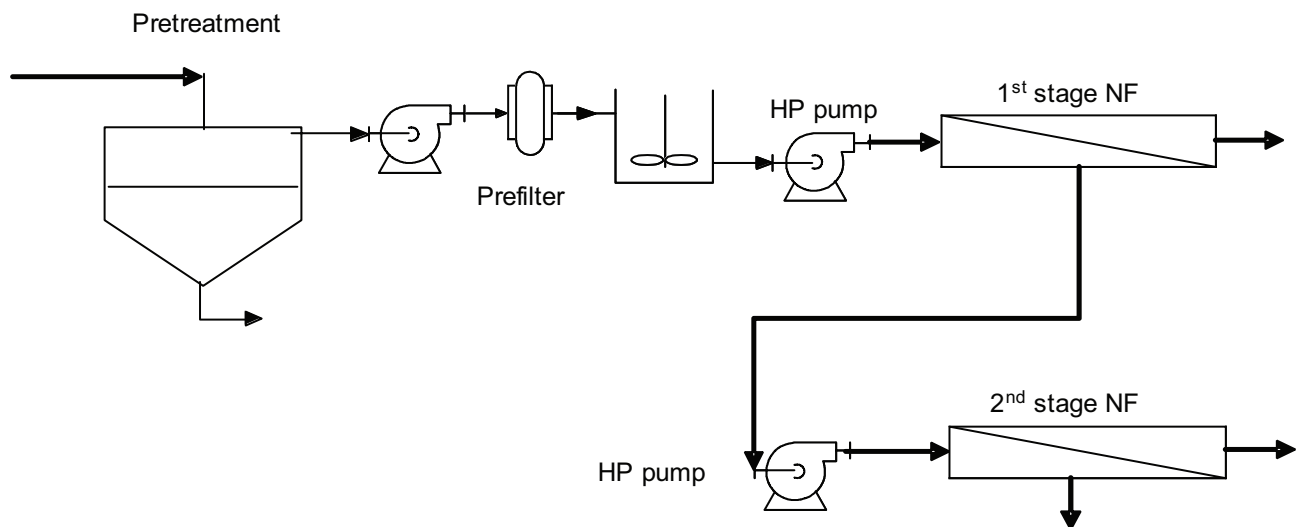

Fig. 1. Schematic diagram of pilot plant for water reuse.

which led to total recovery of 80%. The operation was fully automatic and the electric conductivities were periodically monitored using sensors connected to the feed and permeate sides. The flux, transmembrane pressure (TMP), and pressure drop were measured to analyze the performances of NF membranes and the effect of scale formation.

4. Results and discussion

4.1. Water quality of NF brine and permeate

The concentrations of ionic species in the NF brine and permeate were measured several times during the operation and the average values are summarized in Table 2. Since the recovery of the 1st stage NF was 50%, the 1st stage brine was concentrated by approximately two times. In the 2nd stage, the recovery was 60% and thus the ions were further concentrated to reach the total TDS of 8,718 mg/L in the final brine. The rejections for Ca^{2+} and SO_4^{2-} in the 1st stage were 93.8% and 94.3%, respectively, while those for K^+ and Na^+ were 78.1% and 82.1%, respectively. The rejections for Cl^- and F^- were even lower to show −27.0% and 7.6%, respectively. This is attributed to the Donnan exclusion in NF processes, which leads to the low or negative rejections for monovalent ions in the presence of divalent ions [12,27]. Similar results were obtained in the 2nd stage NF. After the 1st stage NF, the brine showed the $CaSO_4$ saturation degree of 146%, suggesting that the feed water to the 2nd stage NF was already supersaturated and had high scaling potential. After the 2nd stage NF, the brine had the $CaSO_4$ saturation degree of 430%. These results imply that the NF membranes in this pilot plant were exposed to high risk of membrane fouling due to $CaSO_4$ scale formation.

4.2. Effect of scale formation on flux and pressure drop

Fig. 2 shows the variations in permeate flux in the 1st and 2nd stages of the NF processes. Although there are substantial fluctuations in the flux, the 1st stage NF showed relatively a stable performance while the 2nd stage NF resulted in a rapid flux decline after 15 d of the operation. Since the feed water to the 2nd stage NF had high scaling potential in the range of 146% and 430%, it resulted in rapid fouling due to the scale formation. On the other hand, the feed water to the 1st stage NF had lower scaling potential ranging from 58.7% to 146%, the fouling propensity was also lower.

Although the plant was initially set to maintain same TMP, the pressure was varied during the operation. As shown in Fig. 3(a), the inlet and outlet pressures in the 1st stage

NF were almost constant within the first 15 d but suddenly increased after this time. Then, the pressures were reduced by reducing the permeate flux from 35 to 25 L/m² h. This suggests that moderate fouling occurred in the 1st stage NF after the operation of 15 d. The TMP increase more rapidly in
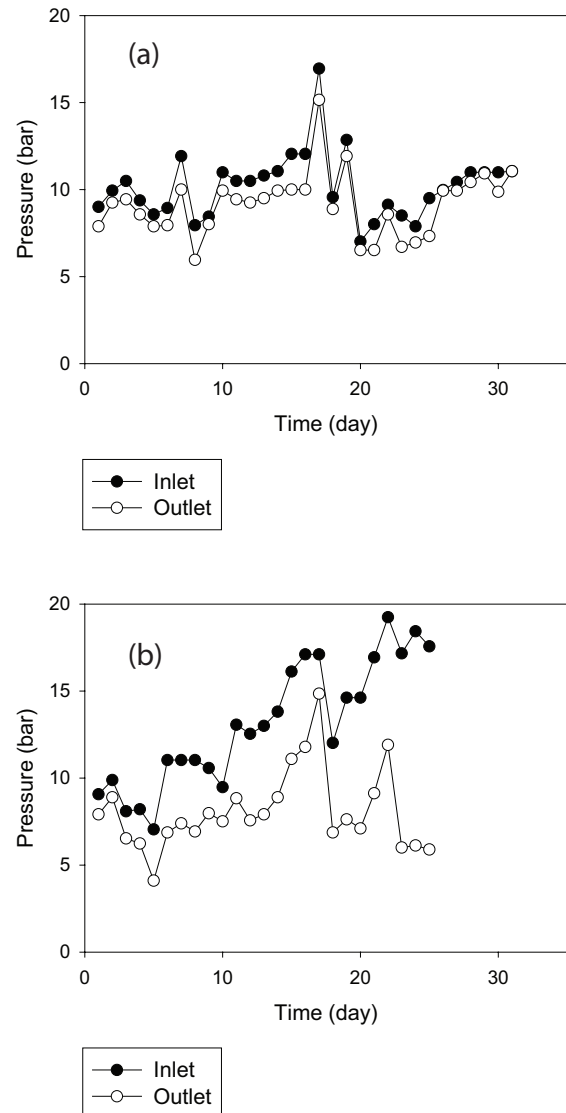

Fig. 3. Changes in inlet and outlet pressures with operation time in the 1st and 2nd stage NF systems. Inlet and outlet pressures in the (a) 1st stage and (b) 2nd stage.

Table 2
Water quality for NF brine and permeate in the 1st and 2nd stages

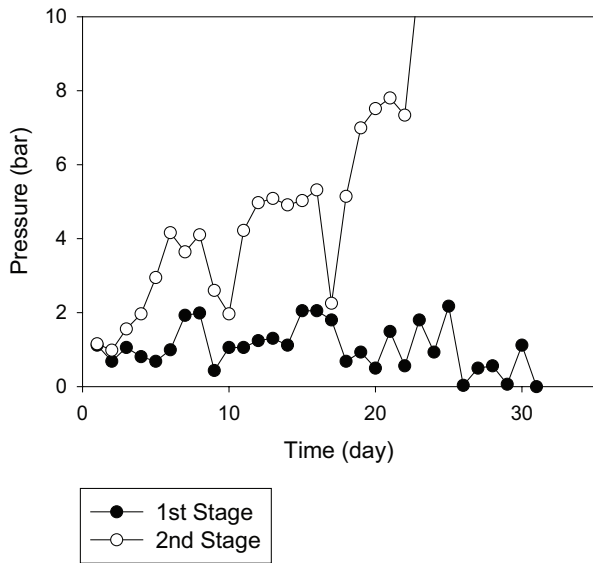|		Ca^{2+} (mg/L)	K^+ (mg/L)	Na^+ (mg/L)	SO_4^{2-} (mg/L)	Cl^- (mg/L)	F^- (mg/L)	TDS (mg/L)
1st stage	Brine	584.2	1,077.6	290.0	3,259.5	86.4	15.7	5,313.4
	Permeate	36.5	235.5	51.8	185.8	109.7	14.5	633.8
	Rejection (%)	93.8	78.1	82.1	94.3	−27.0	7.6	
2nd stage	Brine	812.6	1,727.2	467.6	5,620.0	57.9	32.98	8,718.28
	Permeate	46.5	309.8	91.9	413.6	100.4	21.53	983.73
	Rejection (%)	94.3	82.1	80.3	92.6	−73.4	34.7	

Fig. 4. Changes in pressure drop (ΔP_{loss}) with operation time in the 1st and 2nd stage NF systems.

the 2nd stage NF as illustrated in Fig. 3(b). The inlet pressure increased from the beginning of the operation and reached the maximum pressure of 19 bar. The outlet pressure also increased but was lower than the inlet pressure, indicating that there was a pressure drop inside the membrane elements. In other words, not only the fouling but also the feed channel blocking occurred by the scale formation in the 2nd stage NF, which is attributed to the high scaling potential.

The pressure drops, which were calculated from the difference between the inlet and outlet pressures, for the 1st and 2nd stage NF systems are shown in Fig. 4. In the 1st stage, the average and maximum pressure drops were 1 and 2 bar, respectively, indicating that feed channel was not blocked by the scale formation. In the 2nd stage, the pressure drop continuously increased to exceed 10 bar. Since the pressure drop led to the reduction in the effective TMP, thereby reducing the permeate flux.

4.3. Scale formation mechanisms

To investigate the mechanisms of scale formation in the pilot-scale NF, the model Eqs. (6) and (7) were applied to analyze the NF operation data. Fig. 5 shows the results of the model fit to the NF permeability data using Eq. (6) to examine the surface crystallization mechanisms. Although the plant data had a lot of flocculation, the model matched the overall trends of the permeability data. In the 1st stage, the permeability gradually decreased with time due to relatively slow fouling due to scale formation. In the 2nd stage, the permeability rapidly decreased with time after the operation of 15 d.

Fig. 6 shows the results of the model fit to the NF permeability data using Eq. (7) to examine the cake formation mechanisms. Compared with the surface crystallization model, the bulk crystallization model (Eq. (7)) could not properly explain the changes in the NF permeability in the 2nd stage. The model fit to the operation data was slightly better in the 1st stage using the bulk crystallization model than the surface crystallization model. However, the bulk crystallization could not properly predict the sudden decrease in the permeability in the 2nd stage NF after 15 d. As indicated in Eq. (7), the bulk crystallization model only can explain the gradual decrease in flux or water permeability. However, the permeability in the 2nd stage was rapidly declined and thus could not be interpreted using the bulk crystallization model. This suggests that the fouling in the 2nd stage NF may be attributed to the surface crystallization rather than the bulk crystallization. It is not clear if the fouling in the 1st stage NF followed the surface crystallization mechanism or the bulk crystallization mechanism. Although the current results suggest that the bulk crystallization model fits the operation data better, more experimental evidence may be required to clarify the fouling mechanism in the 1st stage NF.

Fig. 7 shows the model fits to the pressure drop in the 1st and 2nd stage NF systems. Again, a gradual increase in the pressure drop in the 1st stage NF and a rapid increase in the 2nd stage NF could be successfully fitted using the model Eq. (6). Although the surface crystallization was found to be the dominant fouling mechanism in the 2nd stage,
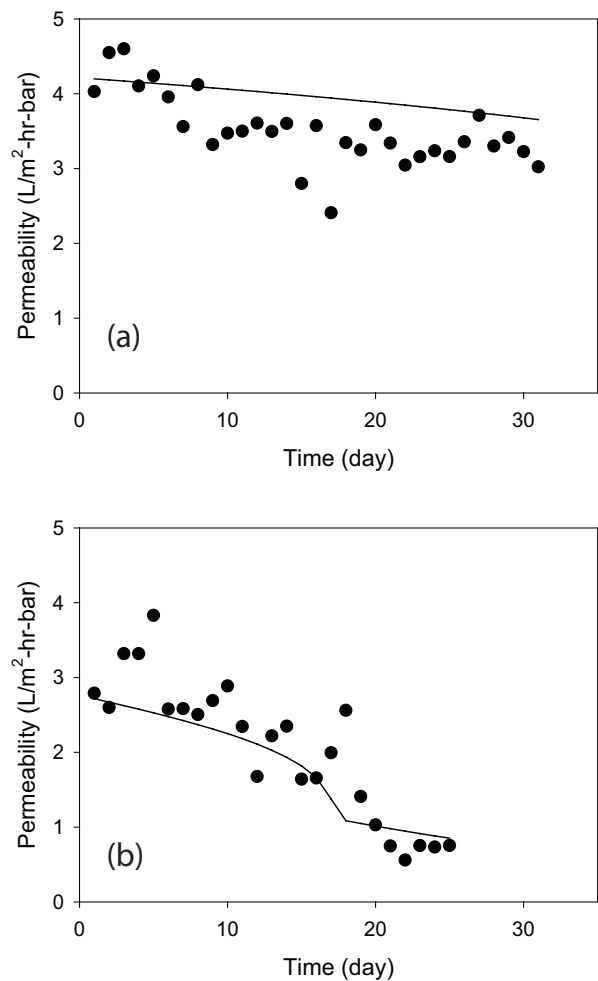

Fig. 5. Comparison of simulated results from the surface blockage model with experimental data for RO permeability ($J/\Delta P$). NF permeability in the (a) 1st stage and (b) 2nd stage.
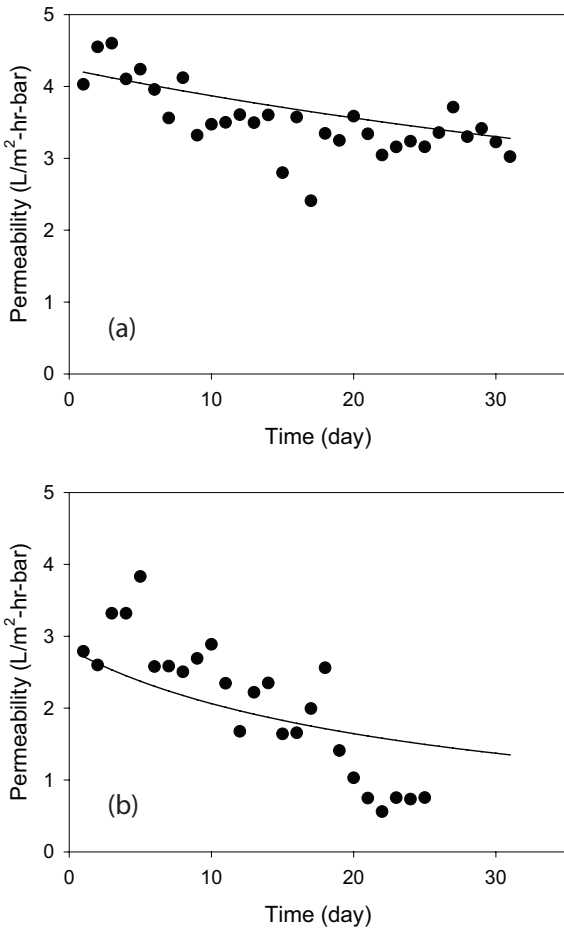
Fig. 6. Comparison of simulated results from the cake formation model with experimental data for RO permeability ($J/\Delta P$). NF permeability in the (a) 1st stage and (b) 2nd stage.
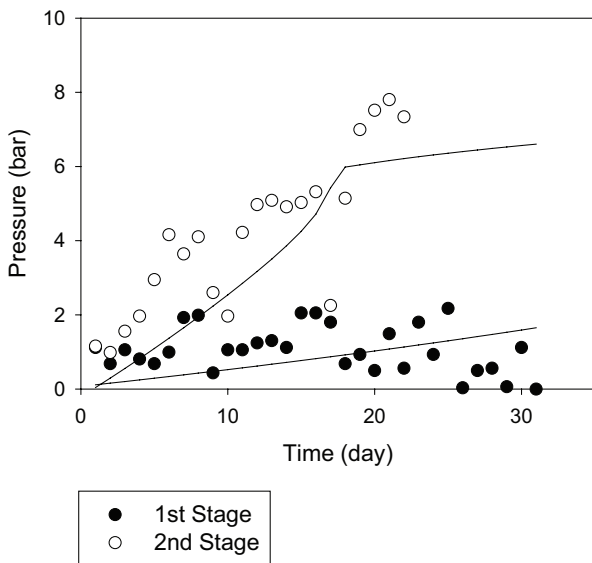
the mechanisms of feed channel blocking include both the surface and bulk crystallization. The particles formed in the bulk solution are recirculated during the NF operation and can result in the blockage of the feed channel. Moreover, the formation of crystals near the membrane surface and feed spacers can also cause the feed channel blockage.

4.4. Changes in local flux and pressures

Although the overall flux can be determined in the plant, it does not show how the local flux is distributed inside the membrane module. Depending on the local flux distribution, fouling and feed channel blockage may occur in specific locations. Accordingly, the longitudinal variations of the local flux, permeability loss, and pressure loss in the membrane modules were analyzed using our model. First, the plant operation data were used as the input for the model. Then, a series of iterations of the model were carried out to find the local profiles to provide the closest results to the plant operation data. These calculations were repeated during the whole operation time. An example of the results of model calculations is given in Fig. 8. The initial flux profile was determined using the initial plant operation data and compared with the profile after 18 d. Initially, the local flux in the 1st stage ranged from 30 to 40 L/m^2 h and that in the 2nd stage ranged from 15 to 35 L/m^2 h. After 18 d, the local flux in the 1st stage showed in the range of 22 and 43 L/m^2 h and that in the 2nd stage ranged from 0 to 45 L/m^{2}h. Since the fouling predominantly occurred in the 3rd element and the 4th element, the local variations of the flux increased in the 2nd stage. It seems that the 4th element cannot produce water since it was completely fouled.

The local progress of NF fouling can be clearly presented by calculating the local permeability. As shown in Fig. 9(a), the relative permeability is 1.0. After 18 d, the relative permeability was significantly reduced in the tail elements as demonstrated in Fig. 9(b). The relative permeability in the 1st

Fig. 7. Comparison of simulated results with experimental data for pressure drop (ΔP_{loss}).
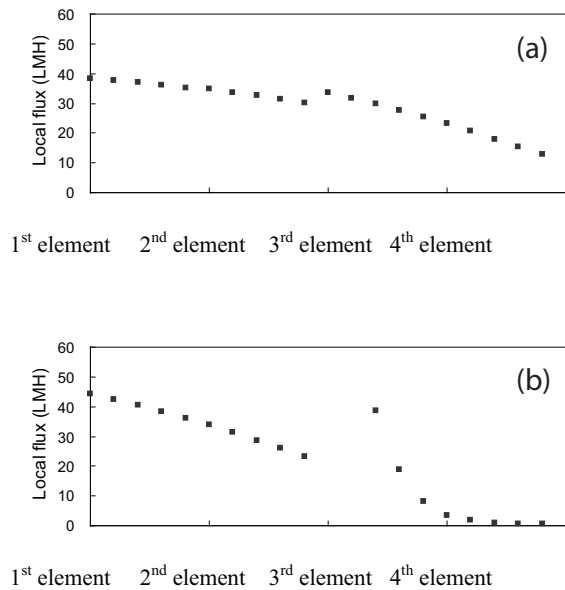

Fig. 8. Changes in local flux profiles with operation time. Local flux at (a) $t = 0$ d and (b) $t = 18$ d.

element was approximately 0.9 but that in the 4th element was approximately zero. Again, it seems that the fouling was moderate in the 1st stage and serious in the 2nd stage.

In addition to the local permeability, the local pressure drop was calculated and the results are shown in Fig. 10. Initially, there was no pressure drop due to the scale formation. After 18 d, the pressure drop was negligible in the 1st element and became noticeable in the 2nd and 3rd elements. The pressure drop was most serious in the 4th element. Although

the applied pressure in the 2nd stage NF after 18 d was 12 bar, the effective TMP in the 4th element ranged from 6 to 9 bar due to the high pressure drop. Accordingly, it should be noted that the control of local permeability loss or local pressure drop is important to control problems related to scale formation.

5. Conclusion

In this study, fouling behaviors of NF membrane elements in a pilot-scale process were examined using the feed water with high scaling potential. The following conclusions were drawn:

- Since the raw wastewater contains high concentrations of Ca^{2+} and SO_4^{2-} ions, gypsum scale formation occurred during the NF processing. Compared with the 1st stage NF, the 2nd stage NF exhibited rapid flux decline as well as an increase in pressure drop.
- The scale formation mechanisms were investigated by applying model equations based on the surface crystallization and bulk crystallization. In the 2nd stage, the fouling mechanism was identified as surface blockage by surface crystallization rather than cake formation by bulk crystallization.
- The longitudinal variations of the local flux, flux, permeability loss, and pressure loss in the membrane modules were analyzed using the model. The model results clearly showed that the tail element in the 2nd stage was seriously fouled after the operation of 18 d. Since this element could not properly produce water, the local flux of the other elements increased to have similar amount of water production from the system.
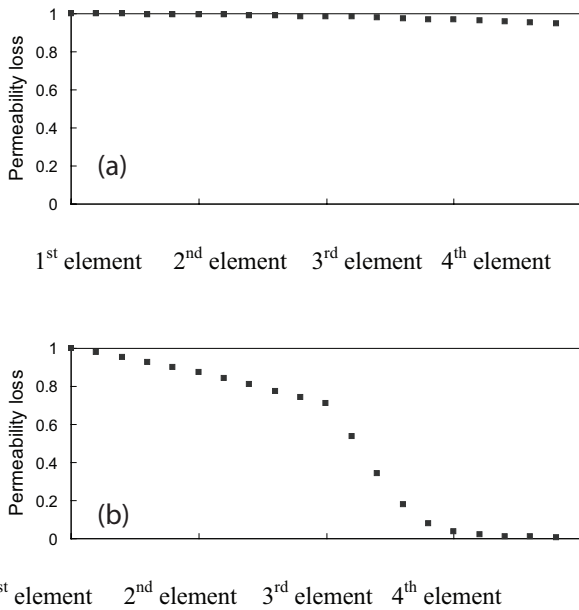

Fig. 9. Changes in local profiles for permeability loss with operation time. Permeability loss at (a) $t = 0$ d and (b) $t = 18$ d.
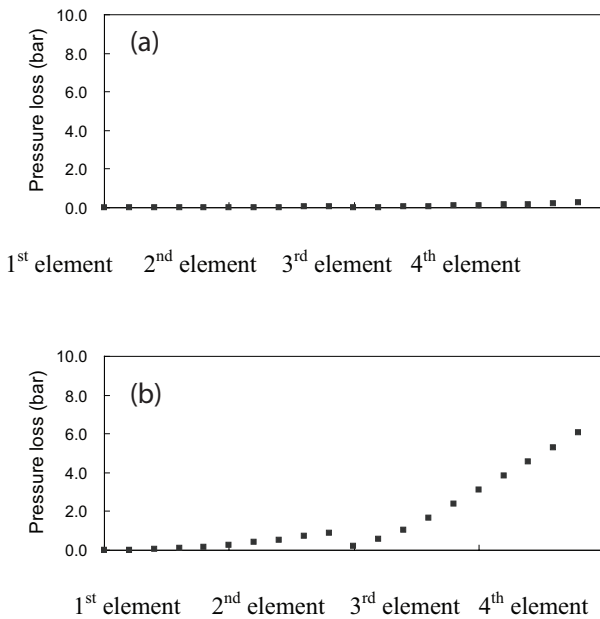
References

[1] A.P.R. Koppol, M.J. Bagajewicz, B.J. Dericks, M.J. Savelski, On zero water discharge solutions in the process industry, Adv. Environ. Res., 8 (2004) 151–171.
[2] L. Pintilie, C.M. Torres, C. Teodosiu, F. Castells, Urban wastewater reclamation for industrial reuse: an LCA case study. J. Cleaner Prod., 139 (2016) 1–14.
[3] J. Wilcox, F. Nasiri, S. Bell, M.S. Rahaman, Urban water reuse: a triple bottom line assessment framework and review, Sustain. Cities Soc., 27 (2016) 448–456.
[4] J.G. Herman, C.E. Scruggs, B.M. Thomson, The costs of direct and indirect potable water reuse in a medium-sized arid inland community, J. Water Process Eng., 19 (2017) 239–247.
[5] S. Lyu, W. Chen, W. Zhang, Y. Fan, W. Jiao, Wastewater reclamation and reuse in China: opportunities and challenges, J. Environ. Sci., 39 (2016) 86–96.
[6] S. Vajnhandl, J.V. Valh, The status of water reuse in European textile sector, J. Environ. Manage., 141 (2014) 29–35.
[7] P. Tram Vo, H.H. Ngo, W. Guo, J.L. Zhou, P.D. Nguyen, A. Listowski, X.C. Wang, A mini-review on the impacts of climate change on wastewater reclamation and reuse, Sci. Total Environ., 494–495 (2014) 9–17.

Fig. 10. Changes in local profiles for pressure drop with operation time. Pressure drop at (a) $t = 0$ d and (b) $t = 18$ d.

[8] C.A. Quist-Jensen, F. Macedonio, E. Drioli, Membrane technology for water production in agriculture: desalination and wastewater reuse, Desalination, 364 (2015) 17–32.

[9] S. Bunani, E. Yörükoğlu, G. Sert, Ü. Yüksel, M. Yüksel, N. Kabay, Application of nanofiltration for reuse of municipal wastewater and quality analysis of product water, Desalination, 315 (2013) 33–36.

[10] J.-H. Tsai, F. Macedonio, E. Drioli, L. Giorno, C.-Y. Chou, F.-C. Hu, C.-L. Li, C.-J. Chuang, K.-L. Tung, Membrane-based zero liquid discharge: myth or reality? J. Taiwan Inst. Chem. Eng., 80 (2017) 192–202.

[11] L.H. Andrade, F.D.S. Mendes, J.C. Espindola, M.C.S. Amaral, Nanofiltration as tertiary treatment for the reuse of dairy wastewater treated by membrane bioreactor, Sep. Purif. Technol., 126 (2014) 21–29.

[12] Z.-Q. Yan, L.-M. Zeng, Q. Li, T.-Y. Liu, H. Matsuyama, X.-L. Wang, Selective separation of chloride and sulfate by nanofiltration for high saline wastewater recycling, Sep. Purif. Technol., 166 (2016) 135–141.

[13] A. Antony, J.H. Low, S. Gray, A.E. Childress, P. Le-Clech, G. Leslie, Scale formation and control in high pressure membrane water treatment systems: a review, J. Membr. Sci., 383 (2011) 1–16.

[14] R. Sheikholeslami, Assessment of the scaling potential for sparingly soluble salts in RO and NF units, Desalination, 167 (2004) 247–256.

[15] A.S. Al-Amoudi, Factors affecting natural organic matter (NOM) and scaling fouling in NF membranes: a review, Desalination, 259 (2010) 1–10.

[16] A.J. Karabelas, Scale formation in tubular heat exchangers—research priorities, Int. J. Thermal Sci., 41 (2002) 682–692.

[17] S. Lee, J. Kim, C.-H. Lee, Analysis of CaSO$_4$ scale formation mechanism in various nanofiltration modules, J. Membr. Sci., 163 (1999) 63–74.

[18] M. Shmulevsky, X. Li, H. Shemer, D. Hasson, R. Semiat, Analysis of the onset of calcium sulfate scaling on RO membranes, J. Membr. Sci., 524 (2017) 299–304.

[19] A.J. Karabelas, A. Karanasiou, S.T. Mitrouli, Incipient membrane scaling by calcium sulfate during desalination in narrow spacer-filled channels, Desalination, 345 (2014) 146–157.

[20] S. Lee, R.M. Lueptow, Control of scale formation in reverse osmosis by membrane rotation, Desalination, 155 (2003) 131–139.

[21] S. Lee, J.-S. Choi, C.-H. Lee, Behaviors of dissolved organic matter in membrane desalination, Desalination, 238 (2009) 109–116.

[22] J.-S. Cho, H. Kim, J.-S. Choi, S. Lee, T.-M. Hwang, H. Oh, D.R. Yang, J.H. Kim, Prediction of reverse osmosis membrane fouling due to scale formation in the presence of dissolved organic matters using genetic programming, Desal. Wat. Treat., 15 (2010) 121–128.

[23] H.-J. Oh, Y.-K. Choung, S. Lee, J.-S. Choi, T.-M. Hwang, J.H. Kim, Scale formation in reverse osmosis desalination: model development, Desalination, 238 (2009) 333–346.

[24] P. Dydo, M. Turek, J. Ciba, K. Wandachowicz, J. Misztal, The nucleation kinetic aspects of gypsum nanofiltration membrane scaling, Desalination, 164 (2004) 41–52.

[25] J.-S. Choi, J.-T. Kim, Modeling of full-scale reverse osmosis desalination system: influence of operational parameters, J. Ind. Eng. Chem., 21 (2015) 261–268.

[26] H.-J. Oh, T.-M. Hwang, S. Lee, A simplified simulation model of RO systems for seawater desalination, Desalination, 238 (2009) 128–139.

[27] J.V. Nicolini, C.P. Borges, H.C. Ferraz, Selective rejection of ions and correlation with surface properties of nanofiltration membranes, Sep. Purif. Technol., 171 (2016) 238–247.